mathematics

MDPI

Article

Numerical Simulation of Shock Wave in Gas–Water Interaction Based on Nonlinear Shock Wave Velocity Curve

Zongduo Wu [1,†], Dapeng Zhang [1,*], Jin Yan [1,2], Jianhua Pang [3] and Yifang Sun [1]

[1] Naval Architecture and Shipping College, Guangdong Ocean University, Zhanjiang 524091, China
[2] Guangdong Provincial Key Laboratory of Intelligent Equipment for South China Sea Marine Ranching, Guangdong Ocean University, Zhanjiang 524091, China
[3] Ocean Intelligence Technology Center, Shenzhen Institute of Guangdong Ocean University, Shenzhen 518055, China
* Correspondence: zhangdapeng@gdou.edu.cn; Tel.: +86-0759-2383007
† Current address: No. 5, Middle Haibin Road, Zhangjiang 524091, China.

Abstract: In a gas–water interaction problem, the nonlinear relationship between shock wave velocity is introduced into a Hugoniot curve, and a Mie–Grüneisen Equation of state (EOS) is established by setting the Hugoiot curve as the reference state. Unlike other simple EOS based on the thermodynamics laws of gas (such as the Tait EOS), the Mie–Grüneisen EOS uses reference states to cover an adiabatic impact relationship and considers the thermodynamics law separately. However, the expression of the EOS becomes complex, and it is not adaptive to many methods. A multicomponent Mie–Grüneisen mixture model is employed in this study to conquer the difficulty of the complex form of an EOS. In this model, some coefficients in the Mie–Grüneisen EOS are regarded as variables and solved using newly constructed equations. The performance of the Mie–Grüneisen mixture model in the gas–water problem is tested by low-compression cases and high-compression cases. According to these two tests, it is found that the numerical solutions of the shock wave under the Mie–Grüneisen EOS agrees with empirical data. When compared to other simple-form EOSs, it is seen that the Mie–Grüneisen EOS has slight advantages in the low-compression case, but it plays an important role in the high-compression case. The comparison results show that the solution of the simple-form EOS clearly disagrees with the empirical data. A further study shows that the gap between the Mie–Grüneisen EOS and other simple-form EOSs becomes larger as the initial pressure and particle velocity increase. The impact effects on the pressure, density and particle velocity are studied. Moreover, the gas–water interaction in a spherical coordinate plane and a two-dimensional coordinate is a significant part of our work.

Keywords: gas–water flow; shock wave; Riemann problem; Mie–Grüneisen mixture model; equation of state (EOS)

MSC: 37M10

Citation: Wu, Z.; Zhang, D.; Yan, J.; Pang, J.; Sun, Y. Numerical Simulation of Shock Wave in Gas–Water Interaction Based on Nonlinear Shock Wave Velocity Curve. *Mathematics* **2024**, *12*, 3268. https://doi.org/10.3390/math12203268

Academic Editors: Joaquim Infante Barbosa and José Alberto Rodrigues

Received: 31 August 2024
Revised: 7 October 2024
Accepted: 8 October 2024
Published: 18 October 2024

1. Introduction

The behavior of shock wave in gas–water flow is an interest of researchers of many fields, such as underwater explosion [1], bubble motion [2], liquid jets, cavitation [3], etc. As the shock wave occurs via an interaction of compressible flow [4], the process of this interaction is always studied using an Euler system. This gas–water problem becomes a so-called "Riemann problem" [5] due to its discontinuous solution. In calculating Riemann problems, the accuracy of the shock wave depends on the numerical method and the equation of state (EOS) [6]. The EOS plays an irreplaceable role in determining the property of materials in an Euler system.

For a gas–water Riemann problem, an ideal gas EOS, which is widely used in the modeling of various gaseous substances, is employed here. Otherwise, there are a number

of different forms of EOSs for water. In the early stage, the EOS of water is expressed in a simple form. Tait EOS [7] is such a typical EOS with brief expression. It has a similar form as an ideal gas EOS and brings convenience to numerical calculation. Another popular EOS for water is stiffened gas EOS [8], which is also written in a simple function. This EOS can be easily coupled with many numerical methods in gas–water interaction, even in recent works [9–13]. The simple forms of an EOS are preferred by researchers because it is much easier to establish Riemann solvers with such an EOS. Nevertheless, some material properties are always ignored by these simple-form EOSs. A modified EOS, named the NASG (Noble Abel Stiffened Gas) EOS [14], is derived from a traditional stiffened gas EOS. The NASG EOS takes temperature into account and is used to describe the thermodynamic properties of water in a specific temperature range. The shock wave problem is based on a set of conservative laws about shock wave parameters [6], wherein the temperature is not a necessary parameter. These conservative laws in terms of shock wave parameters are called the "Hugoniot relationship" [15]. But this relationship is not taken seriously by many EOSs, such as stiffened gas EOS. In addition, the Hugoniot relationship needs to couple with another relationship between shock wave velocity and post-shock particle velocity, whereby the relationship between the two velocities is obtained with experiments. Several decades ago, the LASL (Los Alamos Scientific Laboratory) [16] accumulated a large amount of experimental data under impact and provided particular curves showing the the relationship between shock wave velocity and post-shock particle velocity. This relationship of shock wave and particle velocities is taken as a linear relationship by Miller [17] and introduced into the Mie–Grüneisen EOS. The Mie–Grüneisen EOS can set different reference states to adapt to different material properties [18], and is regarded as a type of general-form EOS, especially for solid and liquid materials. For the Mie–Grüneisen EOS based on the Hugoniot curves, Kerley [19] discussed the validity of the linearity. In this discussion, it is concluded that the expression of the Mie–Grüneisen EOS can be used in a wide variety of materials but it is not absolutely correct.

Water is a common medium, and many researchers study its behavior under impact. Nakayama [20] carried out a shock wave experiment with the help of a gas gun. In this experiment, a series of shock waves parameters are recorded, and the shock wave velocity is defined as a linear function of post-shock particle velocity. However, the ultimate pressure in this experiment is only a little more than 1 Gpa, the effectivity of this linear function under higher pressure is still unknown. LLNL (Lawrence Livermore National Laboratory) [21] provides another representative relationship between shock waves and post-shock particle velocities. This relationship is based on a detonation experiment in water, and a new EOS of water is deduced with the help of this relationship. The LLNL relationship of shock waves and post-shock particle velocities is written in a nonlinear form. However, when it is introduced into the Mie–Grüneisen EOS, the EOS becomes so complex that it is replaced by the stiffened gas EOS [22], even in the latest literature [23]. On the other hand, the EOS for gas also needs to be seriously considered in terms of its applications [24].

In the numerical calculation of the gas–water Riemann problem, it is very complicated to establish a non-oscillation solver for the Mie–Grüneisen EOS due to its complex expression of reference states. As the interface is located between the gas and water, its discontinuity property makes it difficult for researchers to provide an analytic solution for the gas and water [25]. Under this situation, the Mie–Grüneisen mixture model [18] is adaptive. It is considered a whole mixture, and the relative parameters for each phase are considered as a particular parameter of mixture. In the fluid mixture, the interface is identified by a color function, and other parameters are converted to a weighted sum of each fluid component [26]. Comparing with the popular five-equation model by Allaire [27], it is not necessary to consider both the mass fraction and volume fraction in the calculation. Unlike Saurel and Abgrall's multiphase model [28], the conservative laws for each phase do not need to be considered separately. Moreover, it can be well coupled with numerical techniques such as interface tracking [29], grid mapping [30] or some other

limiters [31]. In the previous works, the Mie–Grüneisen mixture model is rarely applied in the study of shock waves. Many research works about shock waves are carried out with the help of commercial software. In this case, a supplement of numerical study becomes very significant. Moreover, the Mie–Grüneisen mixture model can help us to further investigate the performance of different EOSs.

This study seeks an efficient and effective way to simulate the gas-water shock wave problem. When water suffers from outside impact, the dynamic property can be expressed by a nonlinear relationship between the shock wave and particle velocities. Based on the nonlinear relationship, a complex but significant Mie–Grüneisen EOS is derived and used in the numerical calculation of the shock wave problem. The Mie–Grüneisen mixture model is employed here to adapt to such a gas-water two-phase problem. The numerical results are compared with other simple-form EOSs and the effect of the Mie–Grüneisen EOS is given special attention. Afterwards, the performance differences between the Mie–Grüneisen EOS and other EOSs are investigated further. Moreover, the Mie–Grüneisen physical model and numerical model are extended to spherical coordinates, as well as to the 2D problem. During this procedure, the accuracy of calculation is also seriously considered.

2. Basic Theory

2.1. Reference State in Shock Wave Problems

For shock wave problems, it is found in impact experiments that many materials share an approximate relationship between particle velocity u_m and shock wave velocity D [6,8,17,19]:

$$D = c_0 + su_m \tag{1}$$

where c_0 is the speed of sound and s is a coefficient related to the isentropic bulk modules. For a wide range of materials, the linear relation (1) is enough, and the high-order items can be neglected [32]. Certainly, the linear $D - u_m$ relationship is also available for water. However, the linear relationship is not absolutely right, and sometimes, it needs more consideration [19]. To adapt to a strong shock problem (shock pressure more than 10^9 Pa), the relationship of water is described by a nonlinear $D - u_m$ curve given by the Lawrence Livermore National Laboratory (LLNL) [21]:

$$\frac{D - c_0}{u_m} = s_1\left(\frac{u_m}{D}\right) + s_2\left(\frac{u_m}{D}\right)^2 + s_3\left(\frac{u_m}{D}\right)^3 \tag{2}$$

where s_1, s_2 and s_3 are constant coefficients, which are deduced from experimental data. c_0 is the sound speed of static water. The values of s_1, s_2, s_3 and c_0 are given in Table 1. And the Rankine–Hugoniot jump conditions for the conservation of mass, momentum and energy are [17]

$$\begin{cases} \rho = \rho_0 D/(D - u_m) \\ p = p_0 + \rho_0 D u_m \\ e = e_0 + \dfrac{1}{2}(p + p_0)\left(\dfrac{1}{\rho_0} - \dfrac{1}{\rho}\right) \end{cases} \tag{3}$$

where p and e are the pressure and internal energy, respectively. And p_0 and e_0 stand for parameters of initial states. Sometimes, p_0 and e_0 are neglected in strong shock problems. By combining (2) and (3), the Hugoniot state for pressure and energy can be obtained as follows:

$$\begin{cases} p = \dfrac{\rho_0 c_0^2 \mu(1+\mu)}{[1 - (s_1 - 1)\mu - s_2\frac{\mu^2}{\mu+1} - s_3\frac{\mu^3}{(\mu+1)^2}]^2} = p_{ref} \\ e = \dfrac{c_0^2 \mu^2/2}{[1 - (s_1 - 1)\mu - s_2\frac{\mu^2}{\mu+1} - s_3\frac{\mu^3}{(\mu+1)^2}]^2} = e_{ref} \end{cases} \tag{4}$$

where $\mu = \rho/\rho_0 - 1$; p_{ref} and e_{ref} are the pressure and energy of the reference state, and the compression states are defined as points along the Hugoniot curve (as shown in Figure 1 [17]). However, for expansion states, it is hard to describe the reference state by Hugoniot curves due to the negative u_m in the following deduction:

$$\mu = \frac{\rho}{\rho_0} - 1 = \frac{D}{D - u_m} - 1 = \frac{u_m}{D - u_m} < 0$$

since the shock wave travels faster than the interface, so $D - u_m > 0$. As u_m is also a positive value, a conclusion $\mu > 0$ is deduced for the expansion state and this is not real. Therefore, the reference state as (4) is not valid in the expansion phase.

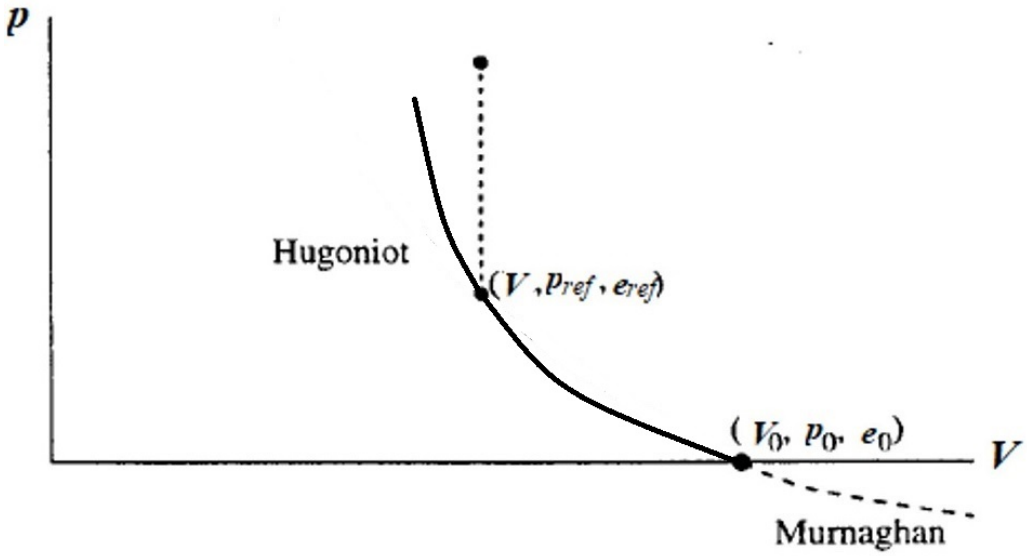

Figure 1. Hugoniot curves. Here, it is taken as the reference state for water.

For the expansion state $\mu < 0$, a Murnaghan isentropic EOS is used here. The compression and expansion states coexist in the same material but exhibit different physical behaviors:

$$\begin{cases} p_{ref} = \left(p_0 + \dfrac{\rho_0 c_0^2}{4s-1}\right)\left(\dfrac{\rho}{\rho_0}\right)^{4s-1} - \dfrac{\rho_0 c_0^2}{4s-1} \\ e_{ref} = e_0 + \displaystyle\int_{V_0}^{V} p_{ref} dV \end{cases} \tag{5}$$

where V denotes volume, and $V = 1/\rho$ [5]. The p_{ref} in (5) is always simplified in a first order of accuracy:

$$\begin{aligned} p_{ref} =& \left(p_0 + \frac{\rho_0 c_0^2}{4s-1}\right)(\mu+1)^{4s-1} - \frac{\rho_0 c_0^2}{4s-1} \\ =& \left(p_0 + \frac{\rho_0 c_0^2}{4s-1}\right)(1 + (4s-1)\mu + o(\mu)) - \frac{\rho_0 c_0^2}{4s-1} \\ =& \rho_0 c_0^2 \mu \end{aligned} \tag{6}$$

Except for cavitation flow, the expansion effect is very weak for liquid water and the variation in volume V can be neglected in the expansion phase, so it is approximately $V = V_0$ and the item $\int p_{ref} dV$ in (5) can be ignored. Thus, there are

$$e_{ref} = e_0 + \int_{V_0}^{V} p_{ref} dV = e_0 \tag{7}$$

Table 1. Parameters of the EOS for water.

C_0	S_1	S_2	S_3	γ_0	α	ρ_0
1480 m/s	2.56	−1.986	0.227	0.5	0	1000 kg/m^3

2.2. Equation of State

In the shock wave problem, the fluids are taken as compressible, and the conservative Euler equation is used to be the basic governing equation:

$$\frac{\partial U}{\partial t} + \frac{\partial F}{\partial x} = 0 \tag{8}$$

where U is a vector of conservative variables, and F represents the fluxes. They can be written as

$$U = \begin{bmatrix} \rho \\ \rho u \\ \rho E \end{bmatrix}, F = \begin{bmatrix} \rho u \\ \rho u^2 + p \\ (\rho E + p)u \end{bmatrix}$$

where E is the total energy and can be deduced by internal energy e and the kinetic energy:

$$E = e + \frac{1}{2}u^2$$

To complete the equation system, an EOS is needed here. For the shock wave problem, the EOS for water and gas must be seriously considered.

As the reference state is known, the EOS can be expressed in a general form:

$$p - p_{ref}(V) = \Gamma(V)(\rho e - \rho e_{ref}(V)) \tag{9}$$

where $V = 1/\rho$. Equation (9) is the Mie–Grüneisen EOS, and Γ is the Grüneisen parameter, which can be simply written as

$$\Gamma = \Gamma_0 \left(\frac{\rho}{\rho_0}\right)^{\alpha} \tag{10}$$

where Γ_0 and α depend on the property of the material. The reference state plays an important role in many physical problems. With the help of e_{ref}, the internal energy of a solid can be considered in two parts: one is a thermal vibrational energy, and another is a potential energy of cold contribution [33]:

$$e(V, T) = e_T(V, T) + e_{ref}(V) \tag{11}$$

the former part of internal energy $e(V, T)$ is in terms of temperature, which has little relationship with the Hugoniot curve. The latter part is defined as the reference state. By setting p_{ref} and e_{ref}, the proportional relationship between thermal pressure p_T and thermal internal energy e_T can be expressed more intuitively. In this case, the pressure can be expressed as

$$\begin{aligned} p(V, T) &= p_{ref}(V) + p_T(V, T) \\ p_T(V, T) &= \frac{\Gamma(V)}{V} e_T(V, T) \end{aligned} \tag{12}$$

Equations (11) and (12) are based on the thermodynamic behavior of crystals. Unlike the Mie–Grüneisen EOS, some other EOSs are derived from the thermodynamics law of gas and do not cover the cold contribution. The reference states provide a convenient way to take care of physical behavior that is not affected by thermodynamics.

Sometimes, the reference states are replaced by other conditions. For example, as an isentropic condition is considered, the internal energy can be written as [34]

$$e(V,S) = e_{ref}(V) + e_S(S) \tag{13}$$

where S is the specific entropy, and Equation (13) can also be used in a water-like substance. In this situation, the pressure p and temperature T satisfy

$$p(V,S) = \frac{\partial e}{\partial V}, T(S) = \frac{\partial e(V,S)}{\partial S} \tag{14}$$

and the derivates of S can be neglected under the constant entropy assumption. Therefore, p can be expressed in a function of ρ:

$$p = B\left[\left(\frac{\rho}{\overline{\rho}}\right)^{\gamma} - 1\right] \tag{15}$$

in which the coefficients for water are as follows: $\gamma = 7$, $B = 3268$ atm, and $\overline{\rho}$ is a constant whose value is 9.233×10^{-4} atm per ft/sec. Equation (15) is the Tait EOS. It can be also regarded as a Mie–Grüneisen EOS form with a constant reference state.

Inserting the reference expressions (4), (11) and (12) into (9), the EOS for water can be written in a piecewise function of p and ρe:

$$\begin{cases} p = \dfrac{\rho_0 c_0^2\left[\mu + (1 - \frac{1}{2}\gamma_0 - \frac{1}{2}a\mu)\mu^2)\right]}{[1 - (s_1 - 1)\mu - s_2\frac{\mu^2}{\mu+1} - s_3\frac{\mu^3}{(\mu+1)^2}]^2} + (\gamma_0 + a\mu)\rho e \quad \mu \geqslant 0 \\ p = \rho_0 c_0^2 \mu + (\gamma_0 + a\mu)\rho e \quad \mu < 0 \end{cases} \tag{16}$$

The EOS for gas is usually derived from the characteristics of ideal gas, which can be written as

$$p = (\gamma - 1)\rho e \tag{17}$$

where the parameter γ is 1.4 for common gas. For special explosive gaseous products with high pressure and temperature, the γ is 3.0 more or less [35].

Moreover, there is another form of EOS, named "stiffened gas EOS". It is derived from a similar behavior of ideal gas [36]:

$$p = (\gamma - 1)\rho e - \gamma p_\infty \tag{18}$$

in which the parameter p_∞ is calculated by the sound velocity c_0:

$$p_\infty = \frac{\rho_0 c_0^2}{\gamma} - p_0 \tag{19}$$

For water, $\gamma = 4.4$, $p_\infty = 6 \times 10^8$. The density ρ of (18) yields the following ratio:

$$\frac{\rho}{\rho_0} = \frac{(\gamma+1)(p + p_\infty) + (\gamma - 1)(p_0 + p_\infty)}{(\gamma+1)(p_0 + p_\infty) + (\gamma - 1)(p + p_\infty)} \tag{20}$$

Although written in a simple form, the determinations of γ and p_∞ are also based on Hugoniot curves. But the relationship $D - u_m$ of the stiffened gas EOS is in a different form (1):

$$D = \sqrt{c_0^2 + \left(\frac{\gamma+1}{4}u_m\right)^2} + \frac{\gamma+1}{4}u_m \tag{21}$$

2.3. Mie–Grüneisen Mixture Model

For such a gas–water problem with the Mie–Grüneisen EOS, a quasi-conservative model, which was proposed by Shyue [18], is employed here. This model is established with respect to the structure of the solution, which includes three characteristics: left wave, right wave and interface.

At the interface position, the structure of the solution shows that density, energy and other material-dependent coefficients are discontinuous across the interface. However, the pressure and particle velocity of each component remain continuous at the interface [8,37], as shown in Figure 2. Otherwise, entropy would be created as soon as the pressures or velocities are different for gas and water [38]. Here, we consider the energy conservative law of (8):

$$\frac{\partial \rho E}{\partial t} + \frac{\partial (\rho E u + p u)}{\partial x} = 0 \tag{22}$$

Then, the EOS (9) can be introduced into (22):

$$\frac{\partial}{\partial t}\left(\frac{p - p_{ref}}{\Gamma} + \rho e_{ref}\right) + u\frac{\partial}{\partial x}\left(\frac{p - p_{ref}}{\Gamma} + \rho e_{ref}\right) = 0$$

and we have

$$\left[\frac{\partial}{\partial t}\left(\frac{1}{\Gamma}\right) + u\frac{\partial}{\partial x}\left(\frac{1}{\Gamma}\right)\right]p + \left[\frac{\partial}{\partial t}\left(\frac{p_{ref}}{\Gamma}\right) + u\frac{\partial}{\partial x}\left(\frac{p_{ref}}{\Gamma}\right)\right] - \left[\frac{\partial}{\partial t}\left(\rho e_{ref}\right) + u\frac{\partial}{\partial x}\left(\rho e_{ref}\right)\right] = 0 \tag{23}$$

Equation (23) is reconstructed using $\partial/\partial\rho$:

$$\left[\frac{\partial \rho}{\partial t} + u\frac{\partial \rho}{\partial x}\right]p\left(\frac{1}{\Gamma}\right)' + \left[\frac{\partial \rho}{\partial t} + u\frac{\partial \rho}{\partial x}\right]\left(\frac{p_{ref}}{\Gamma}\right)' - \left[\frac{\partial \rho}{\partial t} + u\frac{\partial \rho}{\partial x}\right]\left(\rho e_{ref}\right)' = 0 \tag{24}$$

Equation (24) is satisfied under two conditions:

$$\frac{\partial \rho}{\partial t} + u\frac{\partial \rho}{\partial x} = 0 \quad \text{or} \quad p\left(\frac{1}{\Gamma}\right)' + \left(\frac{p_{ref}}{\Gamma}\right)' - \left(\rho e_{ref}\right)' = 0$$

The latter equation above is difficult to satisfy for general problems. It is thus clear that

$$\frac{\partial \rho}{\partial t} + u\frac{\partial \rho}{\partial x} = 0 \tag{25}$$

Here, Equation (25) means that the discontinuous sections move with constant speed u at the interface. According to (25), Equation (23) can be split into three parts:

$$\begin{cases} \dfrac{\partial}{\partial t}\left(\dfrac{1}{\Gamma}\right) + u\dfrac{\partial}{\partial x}\left(\dfrac{1}{\Gamma}\right) = 0 \\ \dfrac{\partial}{\partial t}\left(\dfrac{p_{ref}}{\Gamma}\right) + u\dfrac{\partial}{\partial x}\left(\dfrac{p_{ref}}{\Gamma}\right) = 0 \\ \dfrac{\partial}{\partial t}\left(\rho e_{ref}\right) + u\dfrac{\partial}{\partial x}\left(\rho e_{ref}\right) = 0 \end{cases} \tag{26}$$

Note that the deduction of (25) above is available only at the interface, and the relationship with the left or right wave still needs to be considered.

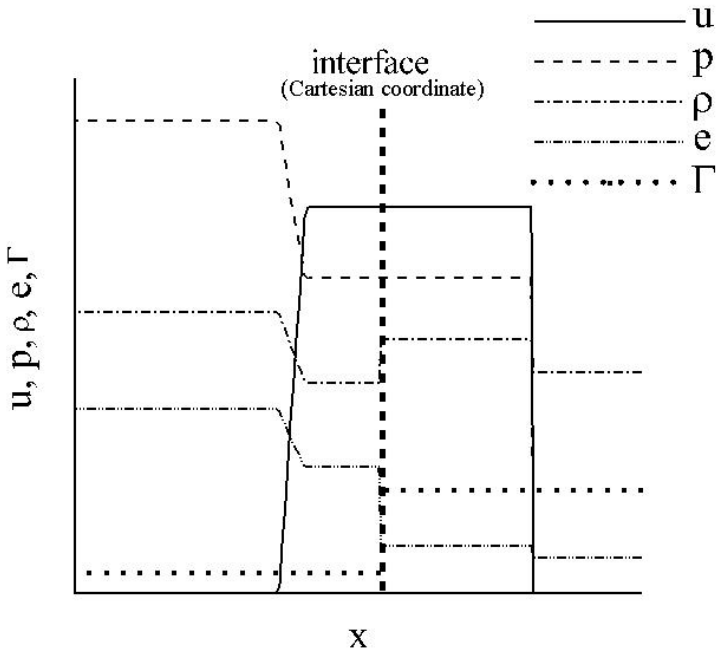

Figure 2. Discontinuous property in Cartesian coordinates. The pressure and velocity maintain equilibrium at the interface, while density and density-dependent parameters are discontinuous.

Meanwhile, at the left/right wave, the pressure and velocity are discontinuous, which means that there is no (25). Note that the left/right wave is separated from the interface and the wave is composed of a single form of fluid, as shown in Figure 3 (a total of five kinds of solutions). In Figure 3, the rarefaction wave corresponds to a weak discontinuity [39]. Thus, the following deduction can be made for $1/\Gamma$:

$$\begin{aligned}\frac{\partial}{\partial t}\left(\frac{1}{\Gamma}\right)+u\frac{\partial}{\partial x}\left(\frac{1}{\Gamma}\right)=&\frac{\partial \rho}{\partial t}\frac{\partial}{\partial \rho}\left(\frac{1}{\Gamma}\right)+u\frac{\partial \rho}{\partial x}\frac{\partial}{\partial \rho}\left(\frac{1}{\Gamma}\right)\\=&\frac{\partial \rho}{\partial t}\left(\frac{1}{\Gamma}\right)'+u\frac{\partial \rho}{\partial x}\left(\frac{1}{\Gamma}\right)'\\=&\left(\frac{1}{\Gamma}\right)'\left(\frac{\partial \rho}{\partial t}+u\frac{\partial \rho}{\partial x}\right)\\=&\left(\frac{1}{\Gamma}\right)'\left(\frac{\partial \rho}{\partial t}+u\frac{\partial \rho}{\partial x}+\rho\frac{\partial u}{\partial x}-\rho\frac{\partial u}{\partial x}\right)\\=&\left(\frac{1}{\Gamma}\right)'\left(\frac{\partial \rho}{\partial t}+\frac{\partial(\rho u)}{\partial x}-\rho\frac{\partial u}{\partial x}\right)=-\left(\frac{1}{\Gamma}\right)'\rho\frac{\partial u}{\partial x}\end{aligned}$$

Thus,

$$\frac{\partial}{\partial t}\left(\frac{1}{\Gamma}\right)+u\frac{\partial}{\partial x}\left(\frac{1}{\Gamma}\right)+\rho\frac{\partial u}{\partial x}\left(\frac{1}{\Gamma}\right)'=0 \tag{27}$$

as in (27)

$$\begin{aligned}\frac{\partial}{\partial t}\left(\frac{p_{ref}}{\Gamma}\right)+u\frac{\partial}{\partial x}\left(\frac{p_{ref}}{\Gamma}\right)+\left(\frac{p_{ref}}{\Gamma}\right)'\rho\frac{\partial u}{\partial x}=0\\\frac{\partial}{\partial t}\left(\rho e_{ref}\right)+u\frac{\partial}{\partial x}\left(\rho e_{ref}\right)+\left(\rho e_{ref}\right)'\rho\frac{\partial u}{\partial x}=0\end{aligned} \tag{28}$$

Compared with Equation (26), Equations (27) and (28) are satisfied at the interface due to the constant u.

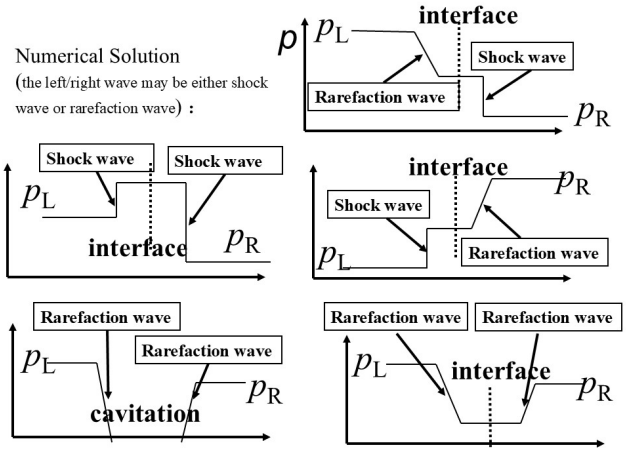

Figure 3. Discontinuous property of solutions.

To summarize (26)–(28), the equations for Γ, p_{ref} and e_{ref} can be written as

$$\begin{cases} \frac{\partial}{\partial t}(\frac{1}{\Gamma}) + u\frac{\partial}{\partial x}(\frac{1}{\Gamma}) + \rho[\frac{\partial}{\partial \rho}(\frac{1}{\Gamma})]\frac{\partial u}{\partial x} = 0 \\ \frac{\partial}{\partial t}(\frac{p_{ref}}{\Gamma}) + u\frac{\partial}{\partial x}(\frac{p_{ref}}{\Gamma}) + \rho[\frac{\partial}{\partial \rho}(\frac{p_{ref}}{\Gamma})]\frac{\partial u}{\partial x} = 0 \\ \frac{\partial}{\partial t}(\rho e_{ref}) + u\frac{\partial}{\partial x}(\rho e_{ref}) + \rho[\frac{\partial}{\partial \rho}(\rho e_{ref})]\frac{\partial u}{\partial x} = 0 \end{cases} \tag{29}$$

for some problems, the analytic forms of Γ, p_{ref} and e_{ref} are always in a complex form, the calculation of (29) can compute parameters Γ, p_{ref} and e_{ref} in an effective way and simplify the computation process.

For a single-component Mie–Grüneisen Riemann problem, the combination of the Euler Equation (8) and auxiliary Equation (29) is enough, while for the multi-phase problem, a transport equation is needed here. As y_g and y_w are used here to represent the mass fraction of gas and water, the transport equation in terms of y_g(or y_w) can be expressed as:

$$\frac{\partial \rho y_w}{\partial t} + \frac{\partial \rho y_w u}{\partial x} = 0 \tag{30}$$

Coupling (29) and (30) with the Euler formulation (8), a mixture model for the gas–water interaction problem can be obtained:

$$\begin{cases} \frac{\partial \rho}{\partial t} + \frac{\partial \rho u}{\partial x} = 0 \\ \frac{\partial \rho u}{\partial t} + \frac{\partial (\rho u^2 + p)}{\partial x} = 0 \\ \frac{\partial \rho E}{\partial t} + \frac{\partial (\rho E + p)u}{\partial x} = 0 \\ \frac{\partial}{\partial t}(\frac{1}{\Gamma}) + u\frac{\partial}{\partial x}(\frac{1}{\Gamma}) + \rho\phi\frac{\partial u}{\partial x} = 0 \\ \frac{\partial}{\partial t}(\frac{p_{ref}}{\Gamma}) + u\frac{\partial}{\partial x}(\frac{p_{ref}}{\Gamma}) + \rho\varphi\frac{\partial u}{\partial x} = 0 \\ \frac{\partial}{\partial t}(\rho e_{ref}) + u\frac{\partial}{\partial x}(\rho e_{ref}) + \rho\psi\frac{\partial u}{\partial x} = 0 \\ \frac{\partial (\rho y_w)}{\partial t} + \frac{\partial (\rho y_w u)}{\partial x} = 0 \end{cases} \tag{31}$$

where the symbols ϕ, φ and ψ denote the derivative functions of the split items $\partial(1/\Gamma)/\partial\rho$, $\partial(p_{ref}/\Gamma)/\partial\rho$ and $\partial(\rho e_{ref})/\partial\rho$, and they are functions in terms of ρ. The derivatives ϕ, φ and ψ are calculated as:

$$\begin{cases} \phi = z_g\left(\frac{1}{\Gamma}\right)_g' + z_w\left(\frac{1}{\Gamma}\right)_w' \\ \varphi = z_g\left(\frac{p_{ref}}{\Gamma}\right)_g' + z_w\left(\frac{p_{ref}}{\Gamma}\right)_w' \\ \psi = z_g\left(\rho e_{ref}\right)_g' + z_w\left(\rho e_{ref}\right)_w' \end{cases} \tag{32}$$

The pressure p is calculated by

$$p = \left(\frac{1}{\Gamma}\right)^{-1}\left[\rho E - \frac{\rho u^2}{2} + \frac{p_{ref}}{\Gamma} - \rho e_{ref}\right]$$

2.4. MUSCL Scheme with Roe Solver

The basic discrete equation in terms of time and space is

$$\frac{U_i^{n+1} - U_i^n}{\triangle t} + \frac{\overline{F}_{i+1/2} - \overline{F}_{i-1/2}}{\triangle x} = 0 \tag{33}$$

where $\triangle t$ and $\triangle x$ are the time step and grid size in x direction. U_i^{n+1} and U_i^n are vectors of conservative variables at the $(n+1)$th and nth time step, $\overline{F}_{i+1/2}$ is the flux between the i and $(i+1)$th cell along the x direction. For the time step $\triangle t$, it is defined as

$$\triangle t = CFL\frac{min(\triangle x)}{max(|u|_i + c_i)} \tag{34}$$

where c_i and u_i represent the particle velocity and sound velocity, respectively. In (34), the convergence conditions are satisfied when $CFL \leqslant 1$. The sound velocity is defined as

$$c^2 = \frac{\partial p}{\partial \rho} + \frac{p}{\rho}\frac{\partial p}{\partial \rho e} = \frac{E + p/\rho - (u^2/2) + p\phi - \varphi + \psi}{1/\Gamma} \tag{35}$$

In the discrete Equation (33), the variable vector U_i is the conservative variable which are listed as:

$$U_i = \left[\rho_i, \rho_i u_i, \rho_i E_i, \frac{1}{\Gamma_i}, \frac{p_{refi}}{\Gamma_i}, \rho_i e_{refi}, \rho_i y_{\mathbf{w}i}\right]^T$$

the fluxes are obtained here by an MUSCL (Monotone Upwind Scheme of Conservation Law)-TVD (Total Variation Diminishing) scheme; and for flux $\overline{F}_{i+1/2}$, there is

$$\begin{aligned} \overline{F}_{i+1/2} = & \frac{1}{2}[F(U_{Li+1/2}) + F(U_{Ri+1/2}) \\ & - \widehat{R}_{i+1/2}\left|\widehat{\Lambda}_{i+1/2}\right|\widehat{L}_{i+1/2}(U_{Ri+1/2} - U_{Li+1/2})] \end{aligned} \tag{36}$$

in which $U_{Li+1/2}$ and $U_{Ri+1/2}$ denote the vector of conservative variables of left and right states. The vectors $F_{Li+1/2}$ and $F_{Ri+1/2}$ can be obtained by

$$\begin{aligned} F_{Li+1/2} &= \left[\rho_{Li}, \rho_{Li}u_{Li}, \rho_{Li}E_{Li}, \frac{1}{\Gamma_{Li}}, \frac{p_{refL_i}}{\Gamma_{Li}}, \rho_{Li}e_{refL_i}, \rho_{Li}y_{\mathbf{w}Li}u_{Li}\right]^T \\ &= U_i + \frac{1}{2}R_{i+1/2}\Phi_{Li+1/2} \\ F_{Ri+1/2} &= \left[\rho_{Ri}, \rho_{Ri}u_{Ri}, \rho_{Ri}E_{Ri}, \frac{1}{\Gamma_{Ri}}, \frac{p_{refR_i}}{\Gamma_{Ri}}, \rho_{Ri}e_{refR_i}, \rho_{Ri}y_{\mathbf{w}Ri}u_{Ri}\right]^T \\ &= U_{i+1} - \frac{1}{2}R_{i+1/2}\Phi_{Ri+1/2} \end{aligned} \tag{37}$$

where $R_{i+1/2}$ is the right eigenvector matrix of $\partial F/\partial U$, which can be expressed as

$$R_{i+1/2} = \begin{bmatrix} 1 & 1 & 1 & & & & \\ u_i - c_i & u_i & u_i + c_i & & & & \\ H_i - u_i c_i & u_i^2/2 & H_i + u_i c_i & p_i & -1 & 1 & \\ \phi_i & & \phi_i & 1 & & & \\ \varphi_i & & \varphi_i & & 1 & & \\ \psi_i & & \psi_i & & & 1 & \\ y_{\mathbf{w}i} & & y_{\mathbf{w}i} & & & & 1 \end{bmatrix} \tag{38}$$

And the items Φ_L and Φ_R in (37) are

$$\begin{aligned} \Phi_{Ri+1/2} &= (I - \frac{\triangle t}{\triangle x}\Lambda_{i+1/2})S_{i+1/2} \\ \Phi_{Li+1/2,j} &= (I + \frac{\triangle t}{\triangle x}\Lambda_{i+1/2})S_{i+1/2} \end{aligned} \tag{39}$$

where Λ is the diagonal matrix of the eigenvalue matrix and can be written as

$$\Lambda_{i+1/2} = \begin{bmatrix} u_i - c_i & & & & & & \\ & u_i & & & & & \\ & & u_i + c_i & & & & \\ & & & u_i & & & \\ & & & & u_i & & \\ & & & & & u_i & \\ & & & & & & u_i \end{bmatrix} \tag{40}$$

and $S_{i+1/2}$ is defined as

$$S_{i+1/2} = minmod\left[L_{i+1/2}DU_{i+1/2}, L_{i+3/2}DU_{i+3/2}\right]$$

where $L_{i+1/2}$ is the left eigenvector of $\partial F/\partial U$, and $DU_{i+1/2} = U_{i+1} - U_i$.

The matrix $L_{i+1/2}$ is

$$L_{i+1/2} = \frac{\Gamma_i}{2c_i^2} \cdot \begin{bmatrix} u_i c_i \xi_i + u_i^2/2 & -u_i - c_i\xi_i & 1 & & \\ -u_i^2 + 2\xi_i c_i^2 & 2u_i & -2 & & \\ -u_i c_i \xi_i + u_i^2/2 & -u_i + c_i\xi_i & 1 & & \\ -\phi_i u_i^2 & 2\phi_i u_i & -2\phi_i & & \\ -\varphi_i u_i^2 & 2\varphi_i u_i & -2\varphi_i & & \\ -\psi_i u_i^2 & 2\psi_i u_i & -2\psi_i & & \\ -y_{\mathbf{w}i} u_i^2 & 2y_{\mathbf{w}i} u_i & -2y_{\mathbf{w}i} & & \\ -p_i & 1 & -1 & & \\ 2p_i & -2 & 2 & & \\ -p_i & 1 & -1 & & \\ 2\phi_i p_i + 2c_i^2\xi_i & -2\phi_i & 2\phi_i & & \\ 2\varphi_i p_i & -2\varphi_i + 2c_i^2\xi_i & 2\varphi_i & & \\ 2\psi_i p_i & -2\psi_i & 2\psi_i + 2c_i^2\xi_i & & \\ 2y_{\mathbf{w}i} p_i & -2y_{\mathbf{w}i} & 2y_{\mathbf{w}i} & 2c_i^2\xi_i & \end{bmatrix} \tag{41}$$

where $\xi = 1/\Gamma$.

In (36), the matrixes $\widehat{\Lambda}_{i+1/2}$, $\widehat{R}_{i+1/2}$ and $\widehat{L}_{i+1/2}$ are defined as the matrixes of the average value of the left and right states. Roe average [5] is a widely used style of average, which can be expressed as

$$\begin{cases} \widehat{u} = \dfrac{\sqrt{\rho_L}u_L + \sqrt{\rho_R}u_R}{\sqrt{\rho_L} + \sqrt{\rho_R}}, \ \widehat{H} = \dfrac{\sqrt{\rho_L}H_L + \sqrt{\rho_R}H_R}{\sqrt{\rho_L} + \sqrt{\rho_R}} \\ \widehat{\xi} = \dfrac{\sqrt{\rho_L}\xi_L + \sqrt{\rho_R}\xi_R}{\sqrt{\rho_L} + \sqrt{\rho_R}}, \ \widehat{\phi} = \dfrac{\sqrt{\rho_L}\phi_L + \sqrt{\rho_R}\phi_R}{\sqrt{\rho_L} + \sqrt{\rho_R}} \\ \widehat{\varphi} = \dfrac{\sqrt{\rho_L}\varphi_L + \sqrt{\rho_R}\varphi_R}{\sqrt{\rho_L} + \sqrt{\rho_R}}, \ \widehat{\psi} = \dfrac{\sqrt{\rho_L}\psi_L + \sqrt{\rho_R}\psi_R}{\sqrt{\rho_L} + \sqrt{\rho_R}} \\ \widehat{p} = \dfrac{1}{\widehat{\xi}}\dfrac{\sqrt{\rho_L}p_L\xi_L + \sqrt{\rho_R}p_R\xi_R}{\sqrt{\rho_L} + \sqrt{\rho_R}} \\ \widehat{c} = \sqrt{\dfrac{1}{\widehat{\xi}}\left[\widehat{H} - (\widehat{u}^2/2) + \widehat{p}\phi - \varphi + \psi\right]} \end{cases}$$

where the corner mark $_L$ and $_R$ represent the variables of left or right states, $H = E + p/\rho$. While for derivatives ϕ, φ and ψ, they have no partial differential items, so the values of $\widehat{\phi}$, $\widehat{\varphi}$ and $\widehat{\psi}$ are defined by the original data of the ith grid point:

$$\widehat{\phi} = \phi_i, \widehat{\varphi} = \varphi_i, \widehat{\psi} = \psi_i$$

A similar style is used to define the Roe average of mass fraction y_w:

$$\rho y_w = \frac{\sqrt{\rho_L}y_{wL} + \sqrt{\rho_R}y_{wR}}{\sqrt{\rho_L} + \sqrt{\rho_R}} \tag{42}$$

However, there is one that detail needs to be emphasized: the parameters of shock wave is affected by the path-conservative effects provided by Dal Maso [40]. There is a slight change, however, if the scheme is different. This property also exists in two-layer shallow water flows [41,42]. The path-conservative problem is analysized in Appendix A. The form of transport equation is also discussed in Appendix A.

3. Numerical Examples

3.1. Weak Shock Problem of Gas–Water Interaction

A simple 1D gas–water interaction problem, which is previously studied by Liu [43], is first considered. The initial states are constituted by gas in the left side, and water in the right side. Their physical parameters are:

$$(\rho, p, u) = \begin{cases} (1270\ \text{kg/m}^3, 8000\ \text{atm}, 0.0) & x \le 0.0 \\ (1000\ \text{kg/m}^3, 1.0\ \text{atm}, 0.0) & x > 0.0 \end{cases}$$

When the time instant t = 0, the gas and water are both in a static state, and the water suffers from a weak impact of gas. Here, the water is described by the Tait EOS, which can provide an analytic solution for this gas–water problem.

In Liu's work, Tait EOS is employed to model the water and is reconstructed by a new form similar to (18): $p = (\gamma - 1)\rho e - \gamma B$. The coefficients of the Tait EOS are listed in Table 2. Our concern is the accuracy of solution when the Tait EOS of water is replaced by the Mie–Grüneisen EOS. On the other hand, the Mie–Grüneisen EOS is founded according to the nonlinear $D - u_m$ relationship as in (2).

Table 2. Initial states of gas and water in a weak shock problem. Both gas and water are initially static.

	p	ρ	EOS
Gas	8000 atm	1.27×10^3 kg/m^3	Ideal Gas EOS
Water	1 atm	1.0×10^3 kg/m^3	Tait EOS

Figure 4 exhibits the curves of density and pressure, as well as the shock velocity position records. From the comparison, it is noticed that the difference between the two kinds of EOSs is minimal. In the pressure curves shown in Figure 4b, the shock wave pressure of the Tait EOS is slightly higher than the Mie–Grüneisen EOS. It seems that the Tait EOS can also achieve excellent solutions even though it is in a simple form. Figure 4c provides the trace of shock sections, which corresponds to the discontinuous sections at the right side of Figure 4a,b. However, the analytic solutions can be easily obtained using the Tait EOS in calculation. Still, it is hard to deduce analytic solutions for the Mie–Grüneisen EOS. Therefore, some other referential data are needed here to check the solution of the Mie–Grüneisen EOS.

Here, the accuracy of shock wave parameters is examined by an empirical formula, which can be expressed as [6]

$$\begin{cases} p_{mx} = \rho_{mx} D u_{mx} \\ u_{mx} = \dfrac{D}{\gamma+1}\left[1 + \dfrac{2\gamma}{\gamma-1}\left(1 - (p_{mx}/p_{CJ})^{\frac{\gamma-1}{2\gamma}}\right)\right] \\ u_{mx} = \sqrt{(p_{mx} - p_0)(V_{mx} - V_0)}, \\ V_{mx} = 1/\rho_{mx} \end{cases}$$

Introducing the relationship (2) into the equation system above, one can obtain the values of p_m, ρ_m, u_m and D by a simple iteration. This approach is used to deduce an approximate solution for D, p_m and u_m, as shown in Table 3. As a reference, the $D - u_m$ relationships cover the experimental data of Nakayama (linear) and LLNL (nonlinear).

Table 3. The contrasts of the density, pressure and shock velocity with approximate solution.

	D (m/s)	p_m (Mpa)	ρ_m (kg/m^3)
Nakayama Linear $D - u_m$ *	1959	494	1146
LLNL Nonlinear $D - u_m$ *	1976	491	1146
Tait EOS	2080	534	1144
Mie–Grüneisen EOS	2084	517	1137

* Approximate iteration solution.

The results of the Mie–Grüneisen mixture model are also presented in Table 3. According to the contrast, it is found that our results are closer to the approximate iteration solutions. It is hard to obtain precise values for shock velocity because the shock section in the numerical results is not in a discontinuous shape, and so the position of the shock is challenging to locate due to the dispersion effects. In our work, the position of the shock is defined by the 200 Mpa pressure level. It is noticed that the density of the shock is only about 1140 kg/m^3, so the compression is not very high in this problem. In this problem, the variation in entropy is nearly unaffected by the compression [34]. A simple-form Tait equation is adequate here based on an isentropic condition.

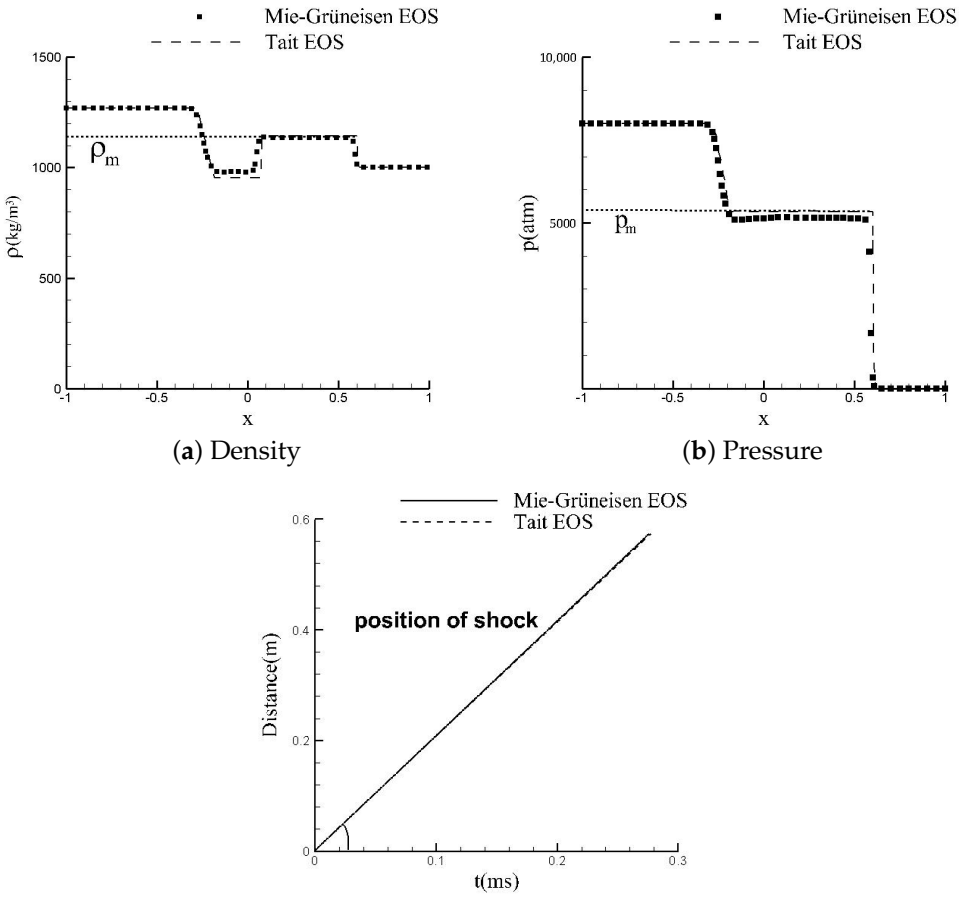

Figure 4. The curves of the density, pressure and shock position in the weak shock problem. The shock wave parameters p_m and u_m are analytic solutions of the Tait EOS. The contrast data of Tait are Liu's numerical solutions. The curves include the following: (**a**) Density. (**b**) Pressure. (**c**) Shock velocity.

3.2. Strong Shock Problem of Gas–Water Interaction

Then, a detonation shock tube problem is used here to test the adaptability of the EOS in a strong shock problem. At $t = 0$, the gaseous detonation product with a C-J (Chapman-Jouguet) state is distributed on the left side. The physical parameters of C-J states are defined as follows [35]:

$$\rho_{\text{C-J}} = \frac{\gamma+1}{\gamma}\rho_0, u_{\text{C-J}} = \frac{\gamma+1}{\gamma}D, p_{\text{C-J}} = \frac{1}{\gamma+1}\rho_0 D^2$$

where ρ_0 = 1630 kg/m^3, $\gamma = 2.727$ and D = 6950 m/s [35]. According to the parameters of C-J states, it can be noticed that the pressure exceeds 10 Gpa (Nakayama's linear data are limited below 1 Gpa) and the gaseous product has an astonishing initial velocity. The EOS group in this example includes the Mie–Grüneisen EOS, Tait EOS, and another stiffened gas EOS of Abgrall. On the other hand, the EOS of gas is also an ideal gas EOS but with a renewed γ.

As three different forms of EOS simulate the gas–water interaction, the empirical values in the first example are used again here. The results of three EOSs are shown in Figure 5. The discontinuous shape of shock waves can be clearly seen in the figure. Nevertheless, significant difference can be found from a comparison of the empirical data. The shock wave parameter calculated by the Tait EOS does not agree well with the empirical data, especially the density ρ. The results indicate that the high-compression problem is complicated to model with the Tait EOS. The Tait EOS is constructed by the property of constant entropy. This property adapts to gas behavior, but it is hard to cover

the Hugoniot relationship under impact. Comparing with the Tait EOS, the adapbility of the stiffened gas EOS is much better in a high-compression problem because the Hugoniot curve is embedded into the foundation of the stiffened gas EOS. However, limited by the simple form of the EOS, the Hugoniot curve is not taken as a reference state; thus, the expressions (18) and (19) only provide a reference state based on initial condition. As there is no condition to set separation as in (11) and (12), the parameters of the shock waves are still not so reliable for the stiffened gas EOS. Both Tait EOS and stiffened gas EOS are affected by the expression form, in which the coefficients cannot contain the compression functions. Thanks to the coefficients p_{ref} and e_{ref}, the Mie–Grüneisen EOS can set a particular ρ function according to detonation experimental curves. In this case, the results of the Mie–Grüneisen EOS are reasonable and close to the empirical data. Due to the complex form of the Mie–Grüneisen EOS, there are slight oscillations at the starting point of the rarefaction waves.

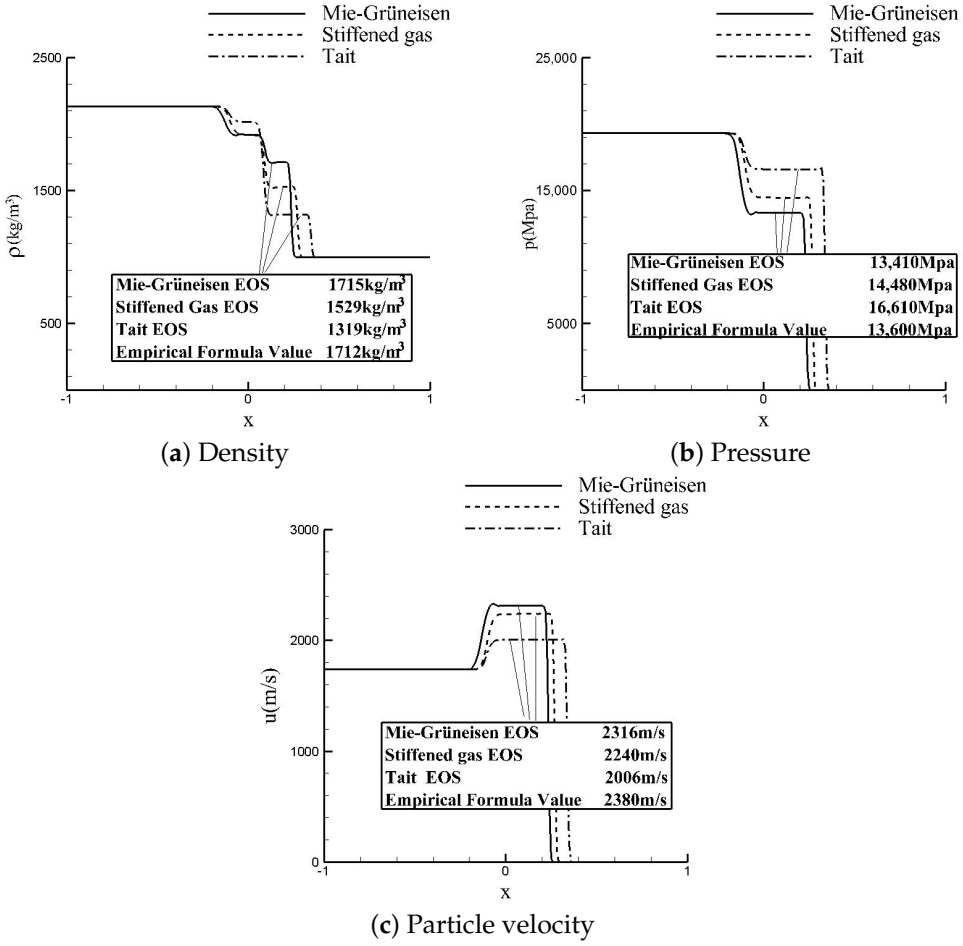

Figure 5. The performances of different EOSs in a strong shock problem. The empirical data are evaluated by the coupling D-u_m curve with C-J parameters. The curves of relative shock parameters are as follows: (**a**) Density. (**b**) Pressure. (**c**) Particle velocity.

3.3. An Investigation of EOS Affection in Gas–Water Interaction

As Tait EOS and stiffened gas EOS are both simple-form equations in which the reference states of Hugoniot curves are not considered, a further study of their performance is carried out here. Here the initial conditions are set to be different to test the adaptability of the Tait EOS and stiffened gas EOS. The difference between the Tait EOS and Mie–Grüneisen EOS and between the stiffened gas EOS and Mie–Grüneisen EOS are presented here. As an extension of the first example, we considered the parameters exhibited in

Figure 5, which include shock density ρ_m, shock pressure p_m and the particle velocity of post shock u_m.

Initially, our attention is paid to the pressure in the initial condition. Two initial densities, 1200 kg/m^3 and 1500 kg/m^3, typical low-compression and high-compression cases, are considered here. The influence of pressure has an effect on the shock parameters, and the variations in ρ_m, p_m and u_m are shown in Figure 6. It can be found that the difference in p_m is the lowest parameter, no matter what EOS is used. The reason is that the EOS expression is always written as a function of pressure. Thus, the pressure is a benchmark parameter and the fitting curves of p are always taken seriously. Conversely, the compression state is represented by the density ρ, but it is not regarded as an essential parameter. There is evidence that the expression of the Tait EOS and stiffened gas EOS only take ρe as a variable and ignore the density ρ. Although the form of EOS is simplified, the density becomes an irrelevant parameter in the expression of EOS. This mistake is very weak when the density variation is small. However, it is amplified when the density becomes large and leads to a depression of impact effects. The results show that the difference among all three parameters maintains an upward trend as the pressure rises. The depression of impact effects cause this phenomenon. As the impact effects are strengthened by the increase in pressure, the compression state is not well described by the Tait EOS and stiffened gas EOS. Comparing with the Tait EOS, the stiffened gas EOS results in less of a difference because it is based on the Hugoniot curve, but the expression form is simplified. Thus, the differences in ρ_m and u_m are both controlled.

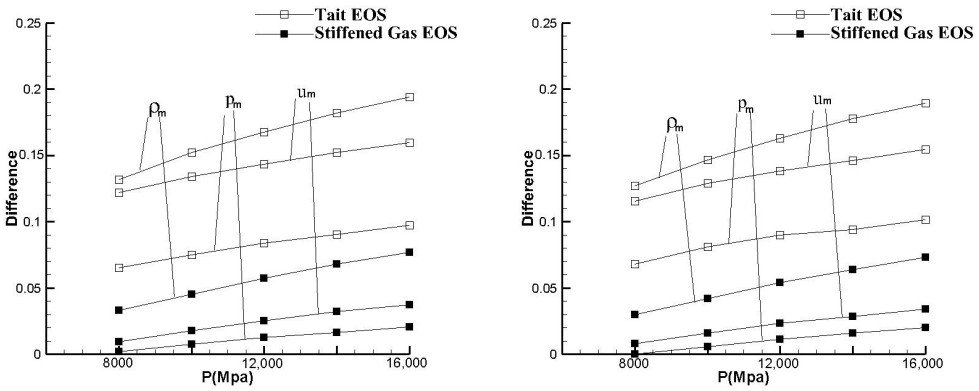

Figure 6. The influence of initial pressure. The difference between the Mie–Grüneisen EOS and Tait EOS and the difference between the Mie–Grüneisen EOS and stiffened gas EOS are distinctly plotted. The initial density of gas is set as follows: (**a**) ρ = 1200 kg/m^3. (**b**) ρ = 1500 kg/m^3.

Next, our attention is transferred to the mechanism of difference when initial velocity ranges from 0 to 1000 m/s. The difference curves are plotted in Figure 7. It is found that the trends of ρ_m, p_m and u_m curves are similar to those in Figure 6. Among the three parameters, the difference in ρ_m is the biggest, while u_m is a little better than ρ_m, p_m has the smallest difference. As u_m increases, the impact effects become larger, and thus the compression of water is enhanced and produces a similar mechanism to that mentioned above. Compared to Figure 6, a gentle slope can be seen in Figure 7. This is because the impact effects that resulting from the variation of u_0 are not strong enough for compression. In Figure 6, the addition of pressure is up to 8000 Mpa. While in Figure 7, by considering that $p = p_0 + \rho_0 D u_m$, the momentum amplification caused by u_0 = 1000 m/s is much lesser than 8000 Mpa (the value of u_m is slightly less than u_0).

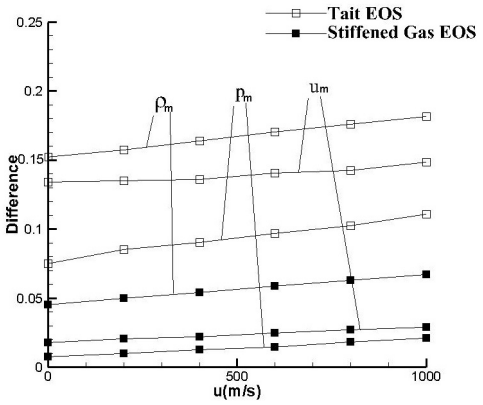

Figure 7. The influence of initial density. The difference between the Mie–Grüneisen EOS and Tait EOS and the difference between the Mie–Grüneisen EOS and stiffened gas EOS are distinctly plotted.

Then, the difference caused by the variation in ρ_0 is considered. Figure 8 presents the difference of ρ_m, p_m and u_m. Unlike p_0 and u_0, the variation in ρ_0 has little relationship with the impact effects when $u_0 = 0$ m/s. In this case, the changes in parameters ρ_m, p_m and u_m are very small, whereby even ρ_0 is up to 1600 kg/m^3 high in value. In addition, the differences in p_m nearly remain constant as the compression increases due to the weak impact. The values of ρ_m and u_m decline slightly. Moreover, the former order of difference ($\rho_m > u_m > p_m$) is also adapted here.

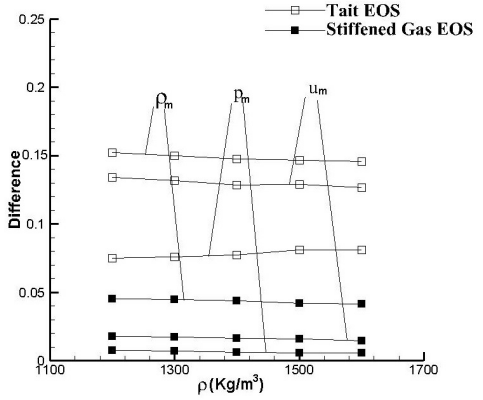

Figure 8. The influence of initial particle velocity. The difference between the Mie–Grüneisen EOS and Tait EOS and the difference between the Mie–Grüneisen EOS and stiffened gas EOS are distinctly plotted.

The results ($\rho_m > u_m > p_m$) in Figures 6–8 are closely related to the structure of real solution. Here, we consider a simple gas–water problem with exact solutions, as in Figure 3. At the interface, the values of p_m and u_m satisfy a characteristic system as follows:

$$\begin{cases} \dfrac{p_m - p_L}{W_L(p_m, p_L, \rho_L)} + (u_m - u_L) = 0 \\ \dfrac{p_m - p_R}{W_R(p_m, p_R, \rho_R)} - (u_m - u_R) = 0 \end{cases}$$

where the function W_L and W_R denote for the left and right waves, respectively. These two functions are determined by the EOS and wave characteristics (shock wave or rarefaction wave), and they have analytic forms when the EOS is either ideal gas EOS or stiffened gas EOS. Such an equation system implies that the p_m can be obtained by an iteration. Then, the value of u_m can be obtained using either equation above. While density is discontinuous at the interface, thus ρ_m can be calculated by a mass conservative law. The relationship among ρ_m, u_m and p_m indicates that ρ_m is affected by D and u_m but ρ_m itself causes no effects to either p_m or u_m. Furthermore, the u_m is affected by p_m, but p_m does not affect u_m.

Therefore, the difference in p_m raises the difference in u_m, then the difference in u_m raises the difference in ρ_m.

3.4. Gas–Water Shock Wave in Spherical System

In this case, a bubble experiment by the LLNL is concerned here [21]. The bubble is generated by the detonation product of 2.1 kg NM (nitromethane) spherical charge, with an initial density of 1.128 g/cm^3. As the charge explodes, a bubble of gaseous product diffuses quickly in water. The computational domain ranges from 0 to 20 $R0$, with 2000 uniform grids in it. $R0$ is the initial radius of the charge.

The numerical calculation is carried out under a spherical coordinate system. The governing equation for the spherical system is reconstructed as [44]

$$\begin{gathered} \frac{\partial \widetilde{U}}{\partial t} + \frac{\partial F(\widetilde{U})}{\partial r} = S(\widetilde{U}) \\ \widetilde{U} = r^2 \cdot U,\ F(\widetilde{U}) = r^2 \cdot F,\ S(\widetilde{U}) = \begin{bmatrix} 0 \\ 2rp \\ 0 \\ 0 \\ 0 \\ 0 \\ 0 \end{bmatrix} \end{gathered} \tag{43}$$

where r denotes the radius. In the new equation system (43), the center point is a singular point because there is no space to construct a discrete equation as (33) and the parameter at the singular point is difficult to evaluate. For the sake of convenience, the parameters at the singularity are defined as the same as the grid point nearby except for the particle velocity. In the center, it is defined as $u = 0$ and other parameters are not affected by any waves.

The movement of the main shock, which is represented by δS, is recorded by camera in this experiment. The shape of the bubble is also investigated in this experiment, and the experimental data contain a record of the radius change δR. The time evolution curves for δS and δR are shown in Figure 9. Compared with the experimental results of δS and δR, it is found that the calculated values become higher as time increases. The reason for the overvalued δS and δR lies in the nonequilibrium of u and p at the interface. As the spherical system is a diffusion system, there is a negative slope rate for real values of p and u at the interface. The sketch of the p and u solution is shown in Figure 10. As a result, the overall decline in u and p ultimately affects the accuracy and increases the strength of the shock wave. Eventually, the values of δS and δR become higher than real, the overvaluation of u and p and becomes larger and larger as distance increases.

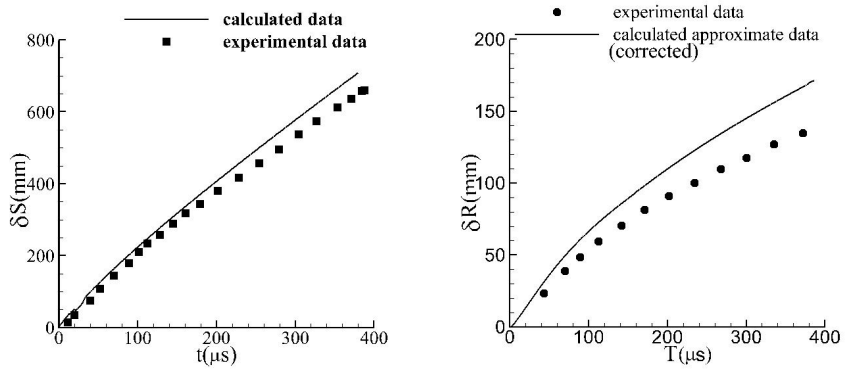

(**a**) Shock wave trace (**b**) Interface trace

Figure 9. The motion of shock and interface in spherical gas–water interaction problem. (**a**) The trace of a shock wave and (**b**) the trace of the interface.

In addition, the disagreement of δR in Figure 9 is slightly larger than δS. This is because the interface of the Mie–Grüneisen mixture model is taken as a diffused interface with thickness, so the exact position of the interface is hard to be defined by such an interface model. The errors of the interface location amplifies as time increases.

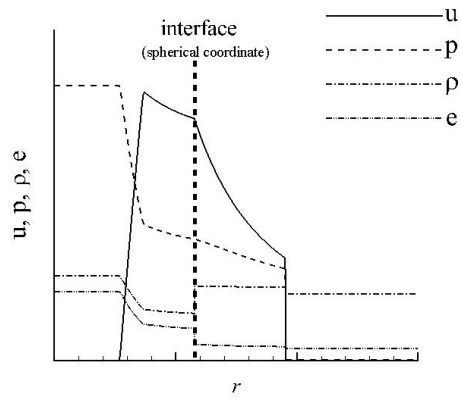

Figure 10. The discontinuous property in spherical coordinates.

In Figure 11, the curves of water density and pressure at instants $t = 200$ and 500 μs are posted. The profiles show the states when the main shock wave travels a long distant. In the beginning, the main shock wave spreads outside. On the other hand, a rarefaction wave moves backwards to the center. The cumulated rarefaction wave then becomes the second shock wave. Afterwards, yielding to the same mechanism, the third shock wave is generated. However, the shock wave generated at the second stage is much lower than the main shock wave, as shown in Figure 11. Regardless, compared with discontinuous parameters such as ρ, ρe, Γ, the velocity and pressure are not constant but are still kept continuous. So, the Mie–Grüneisen mixture model still make sense here.

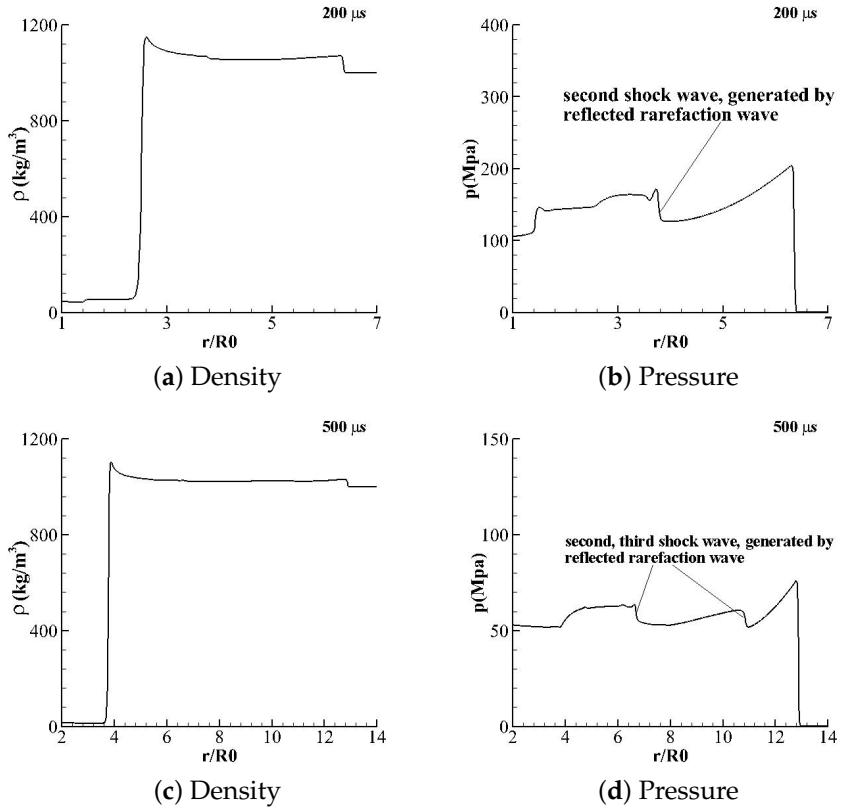

Figure 11. The profiles of density and pressure, respectively: (**a**,**b**) 0.2 ms; (**c**,**d**) 0.5 ms.

3.5. An Extension to the 2D Problem with Three Phases

As the Mie–Grüneisen EOS can adapt to a wide range of materials by setting the expressions of p_{ref} and e_{ref}, it is applied to a 2D problem with three phases. In this example, an underwater explosion phenomenon occurs on the sand bed [45]. So, the shock wave from the explosion not only spreads in water but also penetrates into the sand bed. The explosion charge is in a square shape with a size of 0.15 m. The sand bed is 0.5 m thick, with Mie–Grüneisen coefficients as: ρ_0 = 1950 kg/m^3, $\gamma = 1.28$, s=1.86 and c_0 = 2450 m/s [46]. The bottom of the sand bed is set as a rigid wall. Under the impact, the sand could also be modeled by the Mie–Grüneisen EOS. Here, a linear $D - u_m$ relationship (2) is applied on the sand with coefficients.

Although the gas–water interaction and gas–sand interaction are coupled with each other and the whole interaction becomes complex, it is effective to take the three-phase field as a fluid mixture and use the Mie–Grüneisen mixture model to simulate the interaction process. The pressure contours of this three-phase interaction are given in Figure 12. In contrast, the work of Yao is used here to be a reference [45]. It can be observed that our results are approximate to Yao's results. The discontinuous sections of shock waves in water and in sand are both clearly seen in the contours. The drawback of our results lie in the interface, which is not as distinct as Yao's. This is because the interface is automatically captured and not modified by another procedure.

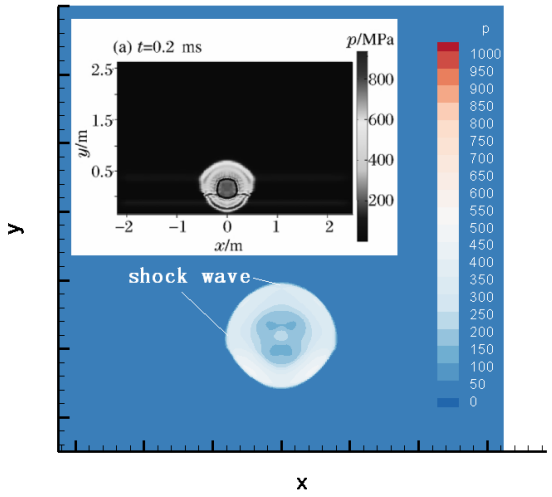

(**a**) 0.2 ms

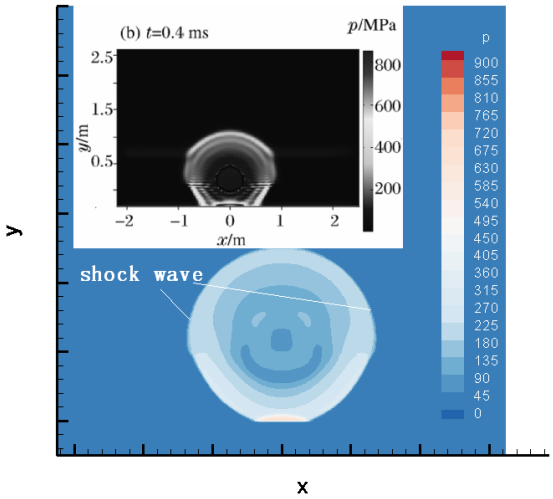

(**b**) 0.4 ms

Figure 12. The comparison of pressure contours in a 2D problem. The contrast contours are copied from Yao's SPH simulation: (**a**) 0.2 ms; (**b**) 0.4 ms.

Figure 13 shows the density distribution contours. It can be seen that the upper parts of the shock wave above the bed spreads freely in the water. On the other hand, another part of the shock wave moves downward and forms reflected shock waves in the sand. The shock wave in the sand is reflected immediately by the rigid wall below the sand. In the center, there is still some gaseous medium left.

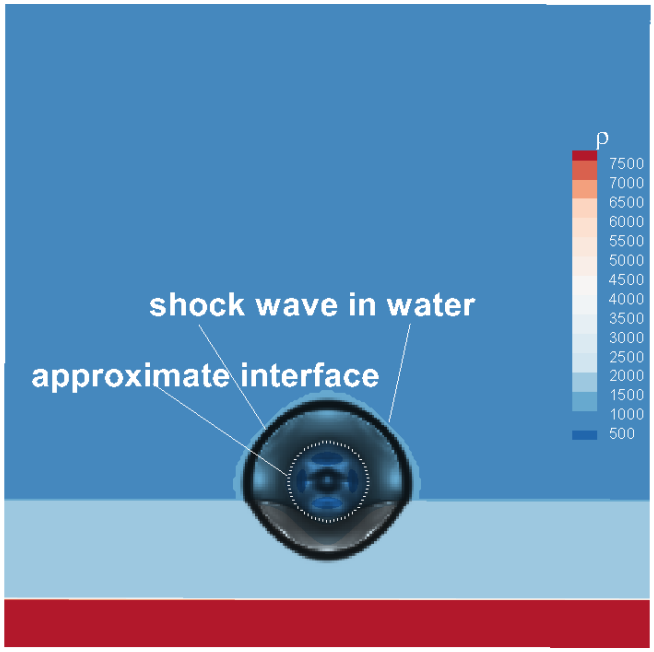

(**a**) 0.2 ms

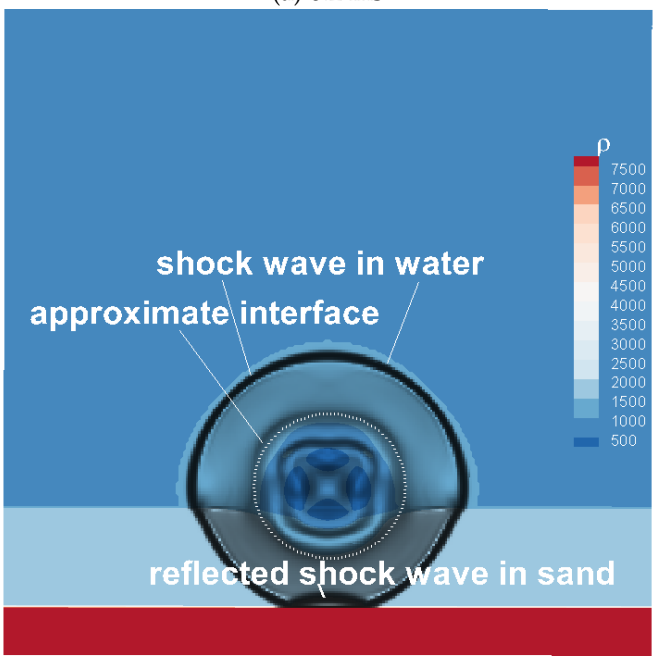

(**b**) 0.4 ms

Figure 13. The density distribution of shock waves in sand: (**a**) 0.2 ms; (**b**) 0.4 ms.

4. Conclusions

According to the calculation of the gas–water shock wave above, some conclusions are summarized as follows:

1. The Mie–Grüneisen mixture model can be applied well in a gas–water interaction and some other multi-phase Riemann problems. The Mie–Grüneisen EOS can rationally

describe the impact effects with the help of the Hugoniot reference state, and achieve precise results that agree well with empirical data.

2. For gas–water problems with low compression, the Mie–Grüneisen EOS does not have any advantage than other simple-form EOSs such as Tait EOS, because the problem can be approximately taken as under an isentropic condition, and a simple-form Tait EOS with a constant reference state is adequate.
3. For gas–water problems with high compression, the results of the Mie–Grüneisen EOS is much better than other simple-form EOSs. With the help of setting reference states as a Hugoniot curve, reliable parameters of shock waves are obtained by the Mie–Grüneisen EOS. The lack of reasonable reference states causes the Tait EOS and stiffened gas EOS to be out of range.
4. The difference between the Mie–Grüneisen EOS and other simple-form EOSs is enlarged by the impact effects of initial conditions. As the initial value of pressure or particle velocity increases, the EOS which is based on a simple isentropic condition (such as Tait EOS) encounters difficulty in describing the impact effects. Other EOSs based on the Hugoniot curve but expressed in a simple form (such as stiffened gas EOS) have some advantages but are still far from the empirical data.
5. Affected by the fundamental theory of an EOS, the deviations of shock wave parameters are different. The order is $\rho_m > u_m > p_m$ from high to low. The reason lies in the calculation process of the three parameters: p_m depends on the medium itself, as well as the initial density and pressure; u_m is affected by p_m according to a couple of characteristic formulas; and lastly, there is ρ_m.
6. The Mie–Grüneisen mixture model can be efficiently applied in a 2D problem, as well as a simple 3D spherical system.

The Mie–Grüneisen mixture model is used to model fluid interaction. It can be extended to fluid–structure interaction by coupling with the finite element method. The calculation of external load can be provided by the Mie–Grüneisen mixture model. On the other hand, this model can be applied to the detonation or combustion phenomena by using the Mie–Grüneisen mixture EOS to model unreacted and reacted substances.

Author Contributions: Conceptualization, Z.W.; methodology, Z.W.; validation, Z.W.; formal analysis, D.Z.; investigation, D.Z.; writing—original draft preparation, Z.W.; writing—review and editing, Z.W. and J.P.; visualization, J.P.; supervision, Y.S.; project administration, J.Y.; funding acquisition, J.Y. All authors have read and agreed to the published version of the manuscript.

Funding: This research was funded by Guangdong Basic and Applied Basic Research (2022A1515011562, 2024A1515012815), Guangdong Provincial Special Fund for promoting high-quality economic development (GDNRC[2021]56, [2021]161), and the National Natural Science Foundation of China (grant number 11702066).

Data Availability Statement: The original contributions presented in the study are included in the article, further inquiries can be directed to the corresponding author.

Conflicts of Interest: The authors declare no conflicts of interest.

Appendix A

Here, we add an appendix to provide an additional numerical test for the Mie–Grüneisen mixture model.

Initially, a mixture shock tube problem with different complex EOSs is considered here. Gaseous explosive and solid copper are placed at the left and right of the shock

tube, respectively. The explosive is modeled by the JWL EOS, which can be written in the Mie–Grüneisen form as

$$\begin{cases} \Gamma = \Gamma_0 \\ p_{ref} = \frac{A_1}{R_1\rho_0}\exp\left(-\frac{R_1\rho_0}{\rho}\right) + \frac{A_2}{R_2\rho_0}\exp\left(-\frac{R_2\rho_0}{\rho}\right) \\ e_{ref} = A_1\exp\left(-\frac{R_1\rho_0}{\rho}\right) + A_2\exp\left(-\frac{R_2\rho_0}{\rho}\right) \end{cases}$$

$$\rho_0 = 1840\,\mathrm{kg/m^3}, \Gamma_0 = 0.25, A_1 = 845.5\,\mathrm{Gpa}, A_2 = 20.5\,\mathrm{Gpa}, R_1 = 4.6, R_2 = 1.35$$

The copper is modeled by the C-C EOS:

$$\begin{cases} \Gamma = \Gamma_0 \\ p_{ref} = B_1\left(\frac{\rho_0}{\rho}\right)^{\varepsilon_1} - B_2\left(\frac{\rho_0}{\rho}\right)^{\varepsilon_2} \\ e_{ref} = -\frac{B_1}{\rho_0(1-\varepsilon_1)}\left[\left(\frac{\rho_0}{\rho}\right)^{\varepsilon_1-1} - 1\right] + \frac{B_2}{\rho_0(1-\varepsilon_2)}\left[\left(\frac{\rho_0}{\rho}\right)^{\varepsilon_2-1} - 1\right] \end{cases}$$

$$\rho_0 = 8900\,\mathrm{kg/m^3}, \Gamma_0 = 2.00, B_1 = 145.67\,\mathrm{Gpa}, B_2 = 147.75\,\mathrm{Gpa}, \varepsilon_1 = 2.99, \varepsilon_2 = 1.99$$

The initial state of the two materials are

$$\begin{cases} \text{explosive} : \rho = 2485.37\,\mathrm{kg/m^3}, p = 37\,\mathrm{Gpa}, u = 0, e = 8149.158\,\mathrm{kJ/kg} \\ \text{copper} : \rho = 8900\,\mathrm{kg/m^3}, p = 1\,\mathrm{atm}, u = 0, e = 117.900\,\mathrm{kJ/kg} \end{cases}$$

Then, the problem is calculated by the Mie–Grüneisen mixture model.

Here, we use different transport equations. One is (30), another is in terms of volume fraction:

$$\frac{\partial z_g}{\partial t} + u\frac{\partial z_g}{\partial x} = 0$$

Taking the different transport equations into account, solutions obtained by conservative and non-conservative transport equations are presented here, as shown in Figure A1. It can be seen that the two results are all very close to the exact solution. No matter whether the transport equations are conservative or not, both of the two results satisfy our needs. In this case, the Mie–Grüneisen mixture model can prevent numerical oscillations and produce accuracy solutions and the interface can be clearly identified by both mass fraction and volume fraction. In Figure A1, the impact of copper generates a leftward rarefaction wave and a rightward shock wave.

In order to explain the path-conservative effects, we take the shock problem of G.M. Ward as an example [31]. The Riemann problem is a single-component impact problem. Initially, the left side of computational zone is the aluminum with compressed state: ρ_L = 4000 kg/m^3, u_L = 2000 m/s, p_L = 7.98 Gpa. The right side is the aluminum with reference state: ρ_R = 2785 kg/m^3, u_R = 0 m/s, $p_R = 0$. The aluminum is modeled by a traditional Mie–Grüneisen EOS with linear relationship (1), in which $\rho_0 = 2785$, c_0 = 5328 m/s, $s = 1.338$, $\gamma_0 = 2.8$, p_0 and e_0 are all set as 0. As the Mie–Grüneisen is used here, the transport equation in terms of y_i can be neglected. We show the influence of the discretization method on the solution, namely using Roe's and Rusanov' schemes. According to the results, it can be found that the two results are absolutely not the same. So, it is known that the parameters can be slightly affected by the schemes. The explanation is that the entropy creation mechanism depends on the schemes. Considering that the approximation effect has a close relation with the path, two different paths are used here. In this case, the numerical solution has a path-conservative property, and different paths would generate different outcomes. The fact is that the schemes converge to different solutions because a discontinuity exists.

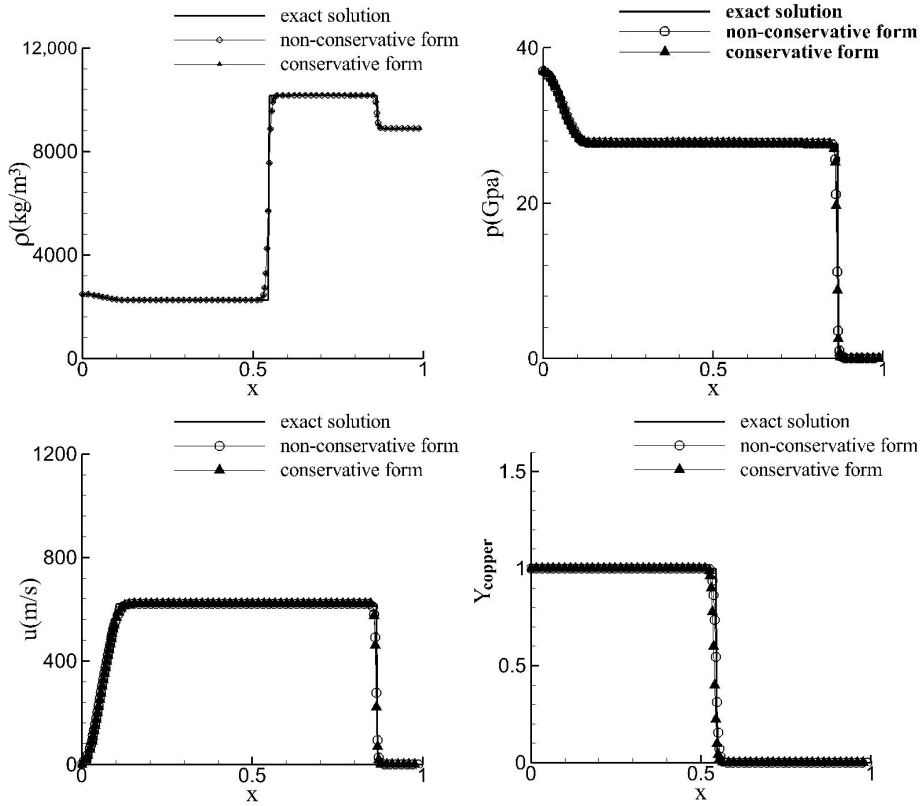

Figure A1. The distribution of mixture density, pressure, velocity and mass fraction (or volume fraction) for an explosive copper shock tube case.

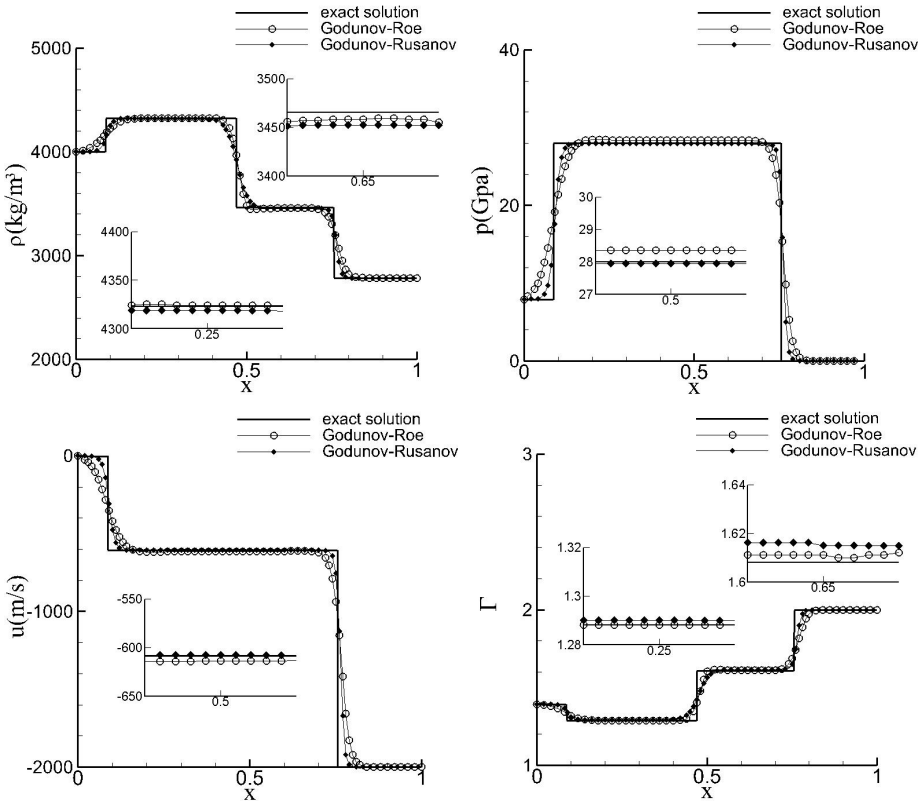

Figure A2. Numerical solution for the aluminum impact problem, including density, pressure, velocity and Γ.

References

1. Cole, R.H. *Underwater Explosion*; Princeton University: Princeton, NJ, USA, 1948.
2. Gilmore, F.R. The collapse and growth of a spherical bubble in a viscous compressible liquid. In *Hydrodynamics Laboratory Report No. 26-4*; California Institute of Technology: Pasadena, CA, USA, 1952.
3. Dellanoy, Y.; Kueny, J.L. Two phase flow approach in unsteady cavitation modeling. In Proceedings of the Cavitation and Multiphase Flow Forum, Toronto, ON, Canada, 4–7 June 1990; p. 98
4. Ren, Y.X. *Basic of Computational Fluid Dynamics*, 1st.; Tsinghua University Press: Beijing, China, 2006; pp. 111–144.
5. Toro, E.F. *Riemann Solvers and Numerical Methods for Fluid Dynamics*, 3rd ed.; University of Trento: Trento, Italy, 2009; pp. 1–24. 115–151. 345–354.
6. Zhang, B.P.; Zhang, Q.M.; Huang, F.L. *Detonation Physics*, 1st.; Weapon Industrial Press: Beijing, China, 2006; pp. 11–28. 336–345
7. Dymond, J.H.; Malhotra, R. The Tait Equation: 100 Years On. *Int. J. Thermophys.* **1988**, *9*, 941–951 [CrossRef]
8. Saurel, R.; Abgrall, R. A simple method for compressible multifluid flows. *SIAM J. Sci. Comput.* **1999**, *21*, 1115–1145. [CrossRef]
9. Yoo, Y.L.; Sung, H.G. Numerical investigation of an interaction between shock waves and bubble in a compressible multiphase flow using a diffuse interface method. *Int. J. Heat Mass Transf.* **2018**, *127*, 210–221. [CrossRef]
10. De Lorenzo, M.; Pelanti, M.; Lafon, P. HLLC-type and path-conservative schemes for a single-velocity six-equation two-phase flow model: A comparative study. *Appl. Math. Comput.* **2018**, *333*, 95–117. [CrossRef]
11. Carmouze, Q.; Saurel, R.; Chiapolino, A.; Lapebie, E. Riemann solver with internal reconstruction (RSIR) for compressible single-phase and non-equilibrium two-phase flows. *J. Comput. Phys.* **2020**, *408*, 109176. [CrossRef]
12. Carmouze, Q.; Fraysse, F.; Saurel, R.; Nkonga, B. Coupling rigid bodies motion with single phase and two-phase compressible flows on unstructured meshes. *J. Comput. Phys.* **2018**, *375*, 1314–1338. [CrossRef]
13. Bai, X.; Li, M. A conservative sharp-interface numerical method for two-dimensional compressible two-phase flows. *J. Sci. Comput.* **2023**, *97*, 30. [CrossRef]
14. Chandran, J.; Salih, A. A modified equation of state for water for a wide range of pressure and the concept of water shock tube. *Fluid Phase Equilibria* **2019**, *483*, 182–188. [CrossRef]
15. Shock Hugoniot. Available online: http://militzer.berkeley.edu/diss/node53.html (accessed on 15 January 2003).
16. Marsh, S.P. *LASL Shock Hugoniot Data*; University of California: Berkeley, CA, USA, 1980.
17. Miller, G.H.; Puckett, E.G. A high-order Godunov method for multiple condensed phases. *J. Comput. Phys.* **1996**, *128*, 110–136. [CrossRef]
18. Shyue, K.M. A Fluid-Mixture Type Algorithm for Compressible Multicomponent Flow with Mie-Gruneisen Equation of State. *J. Comput. Phys.* **2001**, *171*, 678–707. [CrossRef]
19. Kerley, G.I. *The Linear Us-Up Relation in Shock-Wave Physics*; Kerley Technical Services: Appomattox, VA,USA, 2006.
20. Nagayama, K.; Mori, Y.; Shimada, K.; Nakahara, M. Shock Hugoniot compression curve for water up to 1 Gpa by using a compressed gas gun. *J. Appl. Phys.* **2002**, *91*, 476–482. [CrossRef]
21. Steinberg, D.J. Spherical explosion and the equation of state of water. In *Lawrence Livermore National Laboratory Report*; University of California: Livermore, CA, USA, 1987.
22. Hennessey, M.; Kapila, A.K.; Schwendeman, D.W. An HLLC-type Riemann solver and high-resolution Godunov method for a two-phase model of reactive flow with general equations of state. *J. Comput. Phys.* **2020**, *405*, 109180. [CrossRef]
23. Li, Q.; Lv, Y.; Fu, L. A high-order diffuse-interface method with TENO-THINC scheme for compressible multiphase flows. *Int. J. Multiph. Flow* **2024**, *173*, 104732. [CrossRef]
24. Rodio, M.G.; Congedo, P.M.; Abgrall, R. Two-phase flow numerical simulation with real-gas effects and occurrence of rarefaction shock waves. *Eur. J. Mech. B/Fluids* **2014**, *45*, 20–35. [CrossRef]
25. El Idrissi, A.Q. Exact Riemann solver for a nonlinear hyperbolic system of equations modeling a compressible two-phase flow in pipes. *J. Math. Anal. Appl.* **2022**, *505*, 125580. [CrossRef]
26. Saurel, R.; Pantano, C. Diffuse-interface capturing methods for compressible two-phase flows. *Annu. Rev. Fluid Mech.* **2018**, *50*, 105–130. [CrossRef]
27. Saurel, R.; Abgrall, R. A multiphase Godunov method for compressible multifluid and multiphase flows. *J. Comput. Phys.* **1999**, *150*, 425–467. [CrossRef]
28. Allaire, G.; Clerc, S.; Kokh, S. A five-equation model for the Simulation of interfaces between compressible fluids. *J. Comput. Phys.* **2002**, *181*, 577–616. [CrossRef]
29. Shyue, K.M. A wave-propagation based volume tracking method for compressible multicomponent flow in two space dimensions. *J. Comput. Phys.* **2006**, *215*, 219–244. [CrossRef]
30. Shyue, K.M. A high-resolution mapped grid algorithm for compressible multiphase flow problems. *J. Comput. Phys.* **2010**, *229*, 8780–8801. [CrossRef]
31. Ward, G.M.; Pullin, D.I. A hybrid, center-difference, limiter method for simulations of compressible multicomponent flows with Mie-Gruneisen equation of state. *J. Comput. Phys.* **2010**, *229*, 2999–3018. [CrossRef]
32. Ruoff, A.L. Linear Shock-Velocity-Particle-Velocity Relationship. *J. Appl. Phys.* **1967**, *38*, 4976–4980. [CrossRef]
33. Heuzé, O. General form of the Mie-Gruneisen equation of state. *Comptes Rendus Mec.* **2012**, *340*, 679–687. [CrossRef]
34. Flores, J.; Holt, M. Glimm's method applied to underwater explosions. *J. Comput. Phys.* **1981**, *44*, 377–387. [CrossRef]

35. Lee, E.; Finger, M.; Collins, W. JWL equation of states coefficients for high explosives. In *Lawrence Livermore National Laboratory Report*; University of California: Livermore, CA, USA, 1973.
36. Cocchi, J.P.; Saurel, R.; Loraud, J.C. Treatment of interface problems with Godunov-type schemes. *Shock. Waves* **1996**, *5*, 347–357. [CrossRef]
37. Abgrall, R. How to prevent pressure oscillations in multicomponent flow calculations: A Quasi Conservative Approach. *J. Comput. Phys.* **1996**, *125*, 150–160. [CrossRef]
38. Qian, J.; Wang, Y.; Zhang, Y.; Wang, P. An entropy consistent and symmetric seven-equation model for compressible two-phase flows. *J. Comput. Phys.* **2003**, *489*, 112271. [CrossRef]
39. Pandey, M.; Sharma, V.D. Interaction of a characteristic shock with a weak discontinuity in a non-ideal gas. *Wave Motion* **2007**, *44*, 346–354. [CrossRef]
40. Dal Maso, G.; Le Floch, P.; Murat, F. Definition and weak stability of nonconservative products. *J. Math. Pures Appl.* **1995**, *74*, 483–548.
41. Abgrall, R.; Karni, S. Two-layer shallow water system: A relaxation approach. *SIAM J. Sci. Comput.* **2009**, *31*, 1603–1627. [CrossRef]
42. Shah, S.; Hernández-Dueñas, G. Weakly Compressible Two-Layer Shallow-Water Flows Along Channels. *J. Sci. Comput.* **2024**, *100*, 61. [CrossRef]
43. Liu, T.G.; Khoo, B.C.; Yeo, K.S. The simulation of compressible multi-medium flow. I. A new methodology with test applications to 1D gas–gas and gas–water cases. *Comput. Fluids* **2001**, *30*, 291–314. [CrossRef]
44. Liu, T.G.; Khoo, B.C.; Yeo, K.S. The numerical simulations of explosion and implosion in air: Use of a modified Harten's TVD scheme. *Int. J. Numer. Methods Fluids* **1999**, *31*, 661–680. [CrossRef]
45. Yao, X.L.; Yang, W.S.; Chen, J. Numerical calculation of explosion power of mines lying on seabed. *Explos. Shock. Waves* **2011**, *31*, 661–680.
46. Gao, F.; Qiu, Y.Y.; Wang, M.Y. Shock-hugoniot relationships of sand considering porosity evolution. *J. Vib. Shock.* **2017**, *36*, 134–140.